Influence of Technological Manufacturing Conditions on the Porosity of Calcium-Phosphate Scaffolds

Chernobrovchenko V. S.[1*], Dyadyura K. O.[1], Balynskyi M.[1], Panda A.[2]

[1] Sumy State University, 2, Rymskogo-Korsakova St., 40007, Sumy, Ukraine;
[2] Faculty of Manufacturing Technologies with a seat in Prešov, Technical University of Košice, 080 01, Prešov, Slovakia

Abstract. The implantation of bone substitutes depends on the material's osteoconductive potential and the structure's porosity Porosity is a characteristic feature of most materials. The porosity of materials has a strong influence on some of their properties, both structural and functional. An essential requirement for bone scaffolds is porosity, which guides cells into their physical structure and supports vascularization. The macroporosity should be large enough and interdependent for bone ingrowth to occur throughout the entire volume of the implant. The pore size for cell colonization in bioceramics is approximately 100 μm. Pores larger than this value promote bone growth through the material. This pore size allows the flow of growth factors and cell adhesion and proliferation, allowing the formation of new bone and developing the capillary system associated with the ceramic implant. Porosity also affects the rate of resorption of ceramics: the larger the number of micropores, the higher the dissolution rate. The investigated properties were elastic moduli, ultimate strength, compressive strength, and average apparent density. The results obtained in this work are consistent with previous studies, proving the positive role of microporosity in osseointegration and bone formation.

1 Introduction

Bone substitute materials differ in chemical composition, mechanical strength, and biological mechanism of action. Each of them has its advantages and disadvantages. Unfortunately, bone substitutes have not yet achieved optimal mechanical and biological characteristics. Synthetic bone substitutes based on hydroxyapatite and β-tricalcium phosphate are considered today as an adequate alternative to autografts and allografts [1]. Today, when using synthetic materials, a compromise is needed between mechanical and biological characteristics. Since scaffolds are not permanent implants, their primary role is to promote extracellular matrix formation. The relationship between scaffold structure and tissue compatibility has been widely discussed over the past decade. Material properties such as porosity, chemical composition, and geometry alter the relationship between mechanical and biological characteristics, determine interactions with body fluids, and affect the behavior of bone cells.

An essential requirement for bone scaffolds is porosity, which guides cells into their physical structure and supports vascularization [2]. Porosity also affects the rate of the resorption: the larger the number of micropores, the higher the rate of dissolution [3]. As is known, a typical porosity of 90 % and a pore diameter of at least 100 μm are necessary for cell penetration and proper vascularization of the ingrown tissue [4]. The pore size for cell colonization in bioceramics is about 100 μm. Pores larger than 100 microns promote bone growth through the material. This pore size allows the flow of growth factors and cell adhesion and proliferation, allowing for the formation of new bone and developing the capillary system associated with the ceramic implant.

Scaffolds for bone regeneration are synthesized by various methods using a wide range of biomaterials. Research into the integration of biological implants with host tissues is constantly increasing, which leads to the most modern technologies for the manufacture of scaffolds. The superior technology allows the fabrication of complex-shaped frameworks with controlled pore size, shape, and orientation reliably and cost-effectively.

However, natural bone has a unique structure that cannot be reproduced with conventional synthesis methods. The role of micropores in improving the characteristics of bone substitutes has not been studied enough [4]. Not all bone substitutes are equally effective when used as directed. In this regard, biocompatibility risks when using scaffolds from different biomaterials for their intended purpose. Assessing the best options among new technologies (e.g., new chemicals, nanotechnology) is complicated by trade-offs between benefits and risks that are difficult to quantify given the limited and fragmented information available. The introduction of innovations in medical technology should not jeopardize the safety of patients [5]. Risk management and performance assessment processes should be interdependent and regularly updated.

Therefore, the choice of optimal bone substitutes is not always straightforward and largely depends on the clinical application and associated biological and mechanical needs. Research efforts to determine the optimal design of bone substitutes have not led to well-defined solutions [3].

The purpose of this work is to investigate the properties of porous calcium-phosphate bone substitutes depending on the technological conditions of manufacture when changing the process parameters, such as pH, concentration, and calcination temperature, as well as the effect of porosity on physical and mechanical characteristics.

2 Literature Review

Pores in calcium phosphate materials are essential for bone formation as they allow the migration and proliferation of osteoblasts and mesenchymal cells and vascularization. Porous biomaterials are becoming essential in terms of their applications. Pore sizes can range from microscale to macroscale.

In the literature [6], there are independent reviews of theoretical developments of porous materials and their use. For example, in [7], synthetic bone graft substitutes (BGS) have been developed in different pore shapes and sizes using different fabrication technologies.

For almost entirely dense materials with only low residual porosity, it can be assumed with reasonable accuracy that the relationship between properties and porosity is linear. However, for higher porosity, the research results show non-linear correlations. It is expected that the presence of porosity leads to complex laws (not simple direct or inverse linear proportionality). Since the existing references in the literature are somewhat ambiguous in terms of porosity or density, an attempt was made in work to systematize the porosity characteristics of calcium phosphate materials.

Equation (1) [8] is a universal generalization that describes the dependence of the porosity of the investigated properties:

$$p = p_0 \left(1 - \frac{\theta}{\theta_M}\right)^n, \qquad (1)$$

where p is the property of the material with porosity Θ; p_0 is the property for the pore-free material; Θ_M is the maximum porosity of the powder mass, and n is a fitting parameter (positive or negative).

Considering a positive value for n, Equation (1) satisfies the common boundary conditions: $p \to p_0$ as $\Theta \to 0$, and $p \to 0$ as $\Theta \to \Theta_M$, since, in this last situation, interparticle contacts are points. This is the case with most properties analyzed in this paper, including Young's modulus, the electrical and thermal conductivities. If n is negative, $p \to p_0$ as $\Theta \to 0$, and $p \to \infty$ as $\Theta \to \Theta_M$, the typical situation for properties such as the electrical or thermal resistivities or the magnetic coercivity.

Many studies have shown a greater degree and faster rate of ingrowth or attachment of bones with a percentage of porosity; however, there is still some debate about the optimal "type" of porosity. The rate and quality of bone integration are related to pore size, volume fraction of porosity, and the relationship as a function of structural permeability and mechanics.

Gibson and Ashby's paper [9] is the first attempt to revise the properties of porous materials from aspects of their mechanical properties. Ashby calls these materials "cellular" or "lattice" materials, discussing their plastic and brittle mechanical properties in a comprehensive text on the topic, including processing, properties, and uses. Typically, these materials are used as catalyst carriers, filters, and membranes in the chemical, transportation, and energy industries. This use takes advantage of their properties, such as strength-to-weight ratio [6].

Knowledge of elastic properties is critical in the design of intended structural applications:

$$E = E_0 f(\theta, \{c_i\}), \qquad (2)$$

Where E is Young's modulus of the porous material; E_0 is Young's modulus of the solid (pore-free) material; f is a function of Θ and $\{c_i\}$, a set of empirical or fitting parameters sensitive to the microstructural details of the material.

To model the dependence of the shear modulus G on porosity, expressions like expressions for Young's modulus were usually proposed, with the corresponding values of the parameter involved. Parameter Θ_M (maximum porosity) should be the same (since it can be interpreted as the percolation threshold). But the characteristic indicators of Young's modulus and shear modulus do not have to be identical. So, if we assume that Young's modulus is described as follows:

$$E = E_0 \left[1 - \left(\frac{\theta}{\theta_M}\right)\right]^{n_E} \qquad (3)$$

and shear modulus by:

$$E = G_0 \left[1 - \left(\frac{\theta}{\theta_M}\right)\right]^{n_G} \qquad (4)$$

and considering that for homogeneous isotropic materials, Poisson's ratio v can be determined from the moduli E and G as follows:

$$v = \frac{E}{2G} - 1 \qquad (5)$$

substituting equation (3) and (4) into equation (5), we get:

$$\nu + 1 = (\nu_0 + 1)\left[1 - \left(\frac{\theta}{\theta_M}\right)\right]^{n_E - n_G}. \qquad (6)$$

In the specific case, when $nE = nG$ or $nE \approx nG$, then $\nu = \nu_0$ or $\nu \approx \nu_0$. This justifies the experimental results, which indicate a certain insensitivity of Poisson's ratio in porosity for insignificant values of porosity. In practice, there is a difference $nE - nG = 0.09$ for baked iron, which is studied in the porosity range from 0 to 0.22. The model can describe negative values of Poisson's ratio of porous materials when approaching the maximum value of porosity, θ_M (seepage threshold).

In works [10–14], hydroxyapatite frameworks showed higher flexural and compressive strength in the presence of small micropores with an average size of 5 μm compared to 16 μm. Composite frameworks can provide greater rigidity by providing a mechanism to inhibit crack propagation. In the study, the mechanical behavior of porous HA and frameworks with multiscale porosity was evaluated to study the effect of the average micropore size on strength and reliability. The results showed that hydroxyapatite scaffolds with multiscale porosity showed strength (8 MPa) close to the cancellous bone (1–7 MPa). But these figures are lower than the 140-200 MPa range indicated for the cortical bone. The microporous hydroxyapatite framework had better elastic properties than cortical or cancellous bone. The moduli of elasticity of the microporous scaffold with GA from this study (28–30 GPa) were more significant than trabecular (11.4–18.1 GPa) and cortical (15.8–25.9 GPa). For a more accurate correspondence of the modulus of the cortical or trabecular bone, the content of microporosity must be increased by reducing the temperature and sintering time.

Low porosity scaffolds have a large surface area, which is more favorable for initial cell attachment, while high porosity scaffolds may have a lower density, which slows cell proliferation. On the one hand, a higher porosity correlates with an increase in the nutrient diffusion coefficient and a higher hydraulic permeability, but on the other hand, the loss of Young's modulus reduces the mechanical properties of the framework. In addition, the decrease in Young's modulus is higher for biodegradable materials as they lose their integrity upon degradation.

However, this effect may be partially counterbalanced by the newly synthesized extracellular matrix formed within the scaffold, which enhances the overall mechanical strength of the scaffold. Therefore, the porosity value affects both the available surface area and the fluid transfer properties, which must be carefully balanced to obtain an optimized framework [15].

Montazeryan et al. [16] showed that triple periodic minimal structures (that is, a structure whose principal curvature sum is zero at each point [17]) look like promising candidates for frameworks with a high porosity index and transport properties while retaining the corresponding mechanical properties.

Moreover, complex geometries can be achieved, leading to hierarchically organized structures, as shown in Figure 1 [15]. Since the advent of additive manufacturing technologies, triple periodic minimal surfaces (TPMS) have served as a promising tool for designing microstructures due to their superior intrinsic characteristics such as interconnection, tortuosity, and high surface-to-volume ratio. The design space is divided into two or more phases, applying the TPMS equation, resulting in open, periodic porous structures with smooth joints and curvatures. This architecture provided scaffolds with a high degree of fluidity and low modulus of elasticity in the trabecular bone range [16].
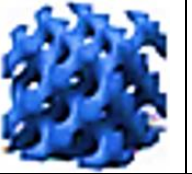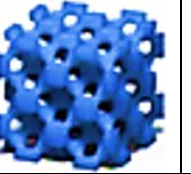
The hydraulic permeability can be calculated using Darcy's law, which relates the velocity V_D of the fluid flowing through the sample, represented in the pressure gradient, to provide the driving force of the flow [15]:

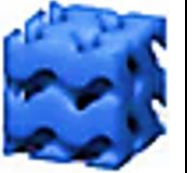$$V_D = -k\frac{\rho g}{\eta}\frac{\Delta h}{H}, \qquad (7)$$

where k is the hydraulic permeability (cm^2); η is the dynamic viscosity of the fluid (Pa·s); H is the sample thickness (cm); ρ is the density of the fluid (g/cm^3); $g = 9.81$ m/s^2 is the gravitational acceleration; Δh is the height difference corresponding to a pressure drop $\Delta P = \rho g \Delta h$.

Table 1 presents examples of triple periodic minimal surfaces (TPMS) unit cell designs with different relative densities as potential scaffolds for tissue engineering.

Table 1 – Examples of TPMS unit cell designs with different relative densities as potential scaffolds for tissue engineering

Porous architecture					
Relative density, %	29	29	33	34	38
Porous architecture					
Relative density, %	51	63	66	66	68

There are various technologies for the manufacture of porous biomaterials. The introduction of new technologies for processing frames made it possible to manufacture individual porous structures with improved mechanical properties (Tables 2–3). A combination of techniques can improve the relationship between processing parameters, the resulting porous microstructures, and the physical, mechanical, and in vitro/in vivo behavior of materials.

Table 2 – Advantages and disadvantages of methods for the manufacture of materials based on hydroxyapatite

Technological method	Characteristics (properties) of porosity	Research results
Partial sintering	Graduated porosity, low interconnection, isotropic structure. As an example, the porosity size is 65 %	[6, 18]
Electro-spinning	When combined with RP, it can create a complex structure, larger pores, oriented fibers; smaller pore size in conventional technologies, low cell infiltration, uneven fiber distribution	[6, 19, 20]
Use of liquid hydrogen/ hydrolysis	High interconnection, directional porosity, fully open porosity, use of organic solvent associated with small pore sizes sometimes show poor homogeneity of the pore structure. Porosity sizes – 47, 56, 45–55 %; pore sizes – 1–10, 90–110 μm	[6, 21]
The method of bubble formation	High porosity, low mechanical strength. Porosity size – 90 %; pore sizes: 1–10, 100, 800 μm	[6, 22, 23]
Gel casting	Almost reticulate, high uniformity, good cohesion combined with foaming. Porosity – 90 %; pore size: 20–1000 μm	[6, 24–26]
Rapid Prototyping (RP) methods	With the possibility of complex shape, the porous structure can be customized according to the host tissue, organic solvents, random microporosity. Porosity – 50–65 %; pore sizes – 700–900, 200–500 μm	[6, 27–31]
Polymer sponge replication	It is possible to create open and interdependent cells, anisotropic pore structure with elongated pores, homogeneity of the suspension. Porosity – 82, 76 %; pore sizes – 700–950 μm, 750–1100 μm	[32, 33]

Table 3 – Manufacturing methods and porosity indices for materials made by various methods

Material	Manufacturing method	Characteristics of porosity	Research results
Polyamide 12/HA	Laser sintering	200–400 μm	[34]
Nanofiber Scaffold (NFS)	Electrospinning	1.5–7.8 μm; 68–93 %	[35]
HA/bioactive glass	Gel casting	100–400 mm; 78 %	[36]
B-TCP	Replication	200–750 mm; approx. 94 %	[37]
HA	3D gel printing	350x350 μm; 52 %	[38]

Rapid prototyping methods allow precise control of porosity characteristics. It is interesting to fabricate hierarchically porous frameworks using methods for fabricating solids of arbitrary shape. The production of scaffolds with a stepped pore size distribution was mainly performed by this method. Polymers are the most studied biomaterials using free-form solid technology. The combination of electrospinning with such technologies has created nanopores next to macropores.

In the technique of partial sintering, the mechanisms of surface diffusion or evaporation-condensation under high-temperature exposure can be predominantly triggered in the composition of particles. This leads to coarsening of the grain/pore without compaction

The size of the original powders can change the porous structure or pore size and morphology, the level of initial compaction, and the following sintering parameters, including pressure, sintering temperature, and time. Microwave sintering and microwave heating can be used to process bioceramic powders. Microwave radiation saves time, energy, and associated processing costs [6, 18].

Electrospinning. In this method, a polymer solution is injected from an electrically conductive needle until it reaches the manifold. High voltage is applied from the end of the die to the manifold, which is fixed away from the die. The electric potential applied to the polymer solution overcomes the surface tension, and drops (tyloric cone) are formed. Polymer jets are ejected from the needle and collected on the manifold. This is how a non-woven and randomly oriented fibrous polymer network with different fiber diameters from 100 nm to several micrometers is obtained, depending on the specific polymer solution and electrospinning parameters. This method cannot control the size of the pores and their location concerning the internal channels [6, 19, 20].

Porosity using a liquid blowing agent. Here, the porogen can be a soluble or insoluble liquid. The resulting structure showed well-defined pore connectivity and directional and fully open porosity, such as lamellar morphology after sintering.

The size of the porosity can be controlled by changing the freezing rate and concentration of the suspensions. The change in the porosity content of lyophilized scaffolds was also studied by changes in parameters such as particle

concentration, the nature of the solvent, and the temperature gradient. The study showed that the thickness of the HA lamella decreased, and the pore width increased with decreasing particle concentration. A decrease in the base temperature from –20 °C to –196 °C created a thinner lamellar microstructure [6, 21].

The bubbling technique is based on mixing the desired components and allows the release of gas bubbles. Gel casting and foaming techniques have been used to create highly porous hydroxyapatite with up to 90% porosity. First, a homogeneous suspension of ceramic powder, water, and monomer solution (i.e., acrylate monomers and methylenebis (acrylamide) monomers) is foamed by adding surfactants. Foaming of suspensions occurs in the in-situ polymerization of organic monomers. Polymerization promoters can be added before shaping. Finally, organic additives are removed at temperatures above 300 °C, and sintering is carried out to consolidate the ceramic frameworks. Porous hydroxyapatite showed spherical interconnected cells ranging in size from 20 to 1000 μm [6, 22, 23].

Gel casting - a method of almost pure form, provides high homogeneity and strength of raw bodies. Powders, organic monomers such as a mixture of methacrylamide and N, N'-methylenebis (acrylamide), binders, dispersants, and solvents are mixed to form a slurry. Then, a crosslinking reaction occurs when an initiator such as ammonium persulfate and a catalyst such as N, N, N ', N'-tetramethylene diamine are added to cause the crude body to polymerize in situ. After evaporation of the solvent, the polymer binds the powders and retains the desired shape. The success of this method depends on the production of well-dispersed and highly solid suspensions (up to 50 vol. %). Dispersant concentration, solids content and mixing time are important factors for the successful implementation of the method [6, 24–26].

Rapid prototyping (RP) or freeform solid specimen fabrication techniques are used to fabricate porous structures. In RP, the digital representation of an object is mathematically broken down into several thin layers. Then the layers are built, merged, and form three-dimensional objects. Examples of RP processes include Stereolithography (STL), Selective Laser Sintering (SLS), Fused Deposition Modeling (FDM), and Direct 3D Printer. They provide control over the fabrication of frameworks with reproducible porosity and specific relationships, geometry, orientation, and pore size due to the particular spatial features of the scaffolds. Direct RP is related to anisotropic shrinkage during manufacturing. To remove the limitation of direct RP, indirect freeform solids production (SFF)/RP was developed for biomaterials, including cast ceramic suspensions. The development of molds, casting methods, and mold stripping is an indirect RP task. The difference between direct RP and indirect RP is that the scaffold is directly produced from biomaterial in the first case, while in the second, the scaffolds are cast and processed in the RP mold. The SL technique has been adapted to manufacture 3D ceramics by adding ceramic powders to light-sensitive resins. This technique, ceramic stereolithography (CSL), requires the preparation of light-sensitive ceramic suspensions [6, 27–31].

A technique uses polymer foam, which is popular in the production of macroporous ceramics and metals. One of the most common synthetic polymeric materials, sponges, which is consumed is polyurethane. The polymer template is moistened several times in a suspension of the corresponding powders to impregnate the templates, and the residues are drained and removed (squeezing out a sponge to get rid of excess suspension). The dried template is then heat-treated to decompose the organic sponges (pyrolysis). After removing the polymer template, ceramic or metal structures are baked at higher temperatures to seal the walls of the posts [32, 33].

3 Research Methodology

3.1 Materials

The chemical formula of hydroxyapatite is $Ca_{10}(PO_4)_6(OH)_2$, and the stoichiometric Ca/P ratio is 1.67 [39]. Bioceramics based on HA are biocompatible, corrosion-resistant, have low toxicity, and have good compressive strength [40]. Whereas β-TCP is bioabsorbable, and bioresorption occurs due to osteoclast activity [41]. An example of porous hydroxyapatite is shown in Figure 1 [42].
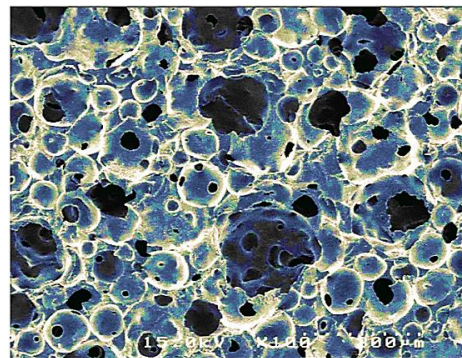

Figure 1 – SEM image of interconnected porous hydroxyapatite (IP-CHA)

Almost all pores are interconnected. HA has mechanical properties: flexural strength, compressive strength, tensile strength, Young's modulus of elasticity, and Vicker's modulus. The hardness values of HA ceramics are in the range of 38–250, 120–150, and 38–300 MPa; 35–120, and 3–7 GPa, respectively [43].

The mass fraction of hydroxyapatite must be at least 95 % of the crystalline phases. The mass fraction of CaO should be no more than 1 % of the crystalline phases. The mass fraction of hydroxyapatite is calculated according to the formula:

$$MF_{HA} = 100\% - MF_{\beta TCP} - MF_{\alpha TCP} - MF_{TTCP} - MF_{CaO}, \quad (8)$$

where MF_{HA} – the mass fraction of crystalline HA; $MF_{\beta TCP}$ – a mass fraction of crystalline βTCP; $MF_{\alpha TCP}$ – a mass fraction of crystalline αTCP; MF_{TTCP} – a mass fraction of crystalline TTCP; MF_{CaO} – a mass fraction of crystalline CaO.

The mass fraction of any phase is considered zero if its value is below the detection threshold [44].

A suspension was prepared with a regulated HA loading. Used cellulose sponges, which can restore their original shape after impregnation and are entirely removed at a temperature of about 600 °C. The cellulose sponges were round samples with a diameter of 1 cm. Hydroxyapatite powder was dissolved in distilled water to obtain a suspension. The powder was gradually placed in water with stirring for uniform dissolution. Then a dispersant in different compositions was added to the solution. Three dispersant compositions were applied to the hydroxyapatite suspensions. After impregnating the slurry, the sponges were dried and heat-treated at 600 °C for 1 hour to remove the organic matrix. The sintering was carried out at 1200 °C for 1 hour.

The influence of three factors (sintering rate, stirring time, and hydroxyapatite concentration) on the porosity, compressive strength, and crystallinity of porous bodies was investigated. For evaluating the sintering rate, samples 1 and 2 were compared. The hydroxyapatite concentration and stirring time were kept constant while the sintering rate was varied. The sizes and weights of all samples were measured before and after heat treatment (Table 4).

Table 4 – Conditions for obtaining porous HA

Sample	Water, g	Concentration of HA, wt. %	Stirring time, min	Sintering speed, °C/h
S1	15.7	44	20	1500
S2	15.7	44	20	220
S3	16.7	42	20	220
S4	16.7	42	4	220
S5	20.0	38	20	220
S6	20.0	38	4	220

3.2 Methods

As already mentioned, the ingrowth of bone substitutes also depends on the porosity of the structure. The macroporosity must be large and interdependent for ingrowth to occur throughout the entire volume of the implant. Porosity affects the rate of resorption of ceramics: the larger the number of micropores, the higher the dissolution rate. The formula calculates the porosity:

$$P = 100 \left(1 - \frac{d_r}{d_{th}}\right), \qquad (9)$$

where P is the degree of porosity, %; d_r – calculated by measuring the size and weight of a parallelepiped bone substitute with a minimum volume of 2 cm³. The volume V of the bone substitute is calculated using the measured parameters and then determine d_r by the formula:

$$d_r = \frac{m}{V}; \qquad (10)$$

d_{th} – insurance for formula insurance for a formula:

$$d_{th} = \frac{d_{HAP}\frac{MF_{HA}}{d_{HA}} + d_{\beta TCP}\frac{MF_{\beta TCP}}{d_{\beta TCP}}}{\frac{MF_{HA}}{d_{HA}} + \frac{MF_{\beta TCP}}{d_{\beta TCP}}}. \qquad (11)$$

Young's modulus E_s of cellular materials is defined as follows:

$$E_s = E_b \left(\frac{\rho_s}{\rho_b}\right)^2, \qquad (12)$$

where E_b – Young's modulus of the bulk material [26].

4 Results and Discussion

As can be seen from Figure 2 (sample 1) was found to have a high average apparent density, compressive strength, and Young's modulus, while the average porosity was lower. The average compressive strength for sample 1 was 10 MPa, the average apparent density was 2.03 g/cm³, and the average porosity was 35.9 %. It was found experimentally that a higher rate of sintering speed leads to higher apparent density and high compressive strength.
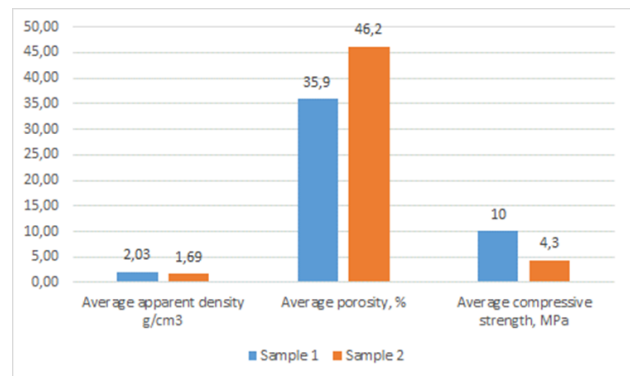

Figure 2 – Average visible density, compressive strength, and porosity of samples 1 and 2

The effect of the mixing period was evaluated by comparing samples 3 and 4, as well as samples 5 and 6. The preparation conditions are shown in Table 3, physical properties – in Table 5.

Figure 3 shows a comparison of samples 3, 4, 5, and 6 in terms of their average apparent density, compressive strength, and porosity. Comparing samples 3 and 4 shows that an increase in the mixing time increased the compressive strength and apparent density but decreased the porosity. The same can be done for samples 5 and 6. Increasing the mixing time leads to the destruction of agglomerates, and the resulting suspension becomes more homogeneous. The relationship of these parameters is shown graphically in Figure 4 a–c.

Table 5 – Conditions for preparation of hydroxyapatite and physical properties of porous samples S1, S2, S3, S4, S5 and S6

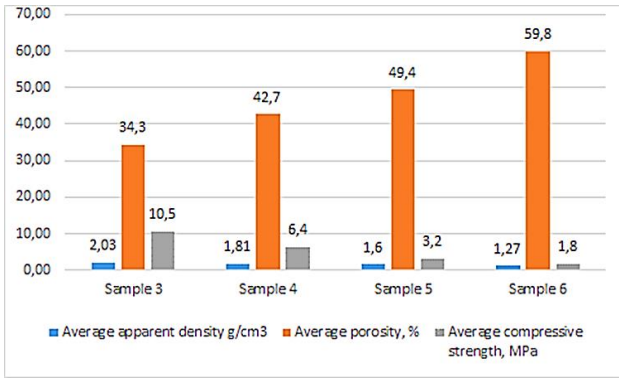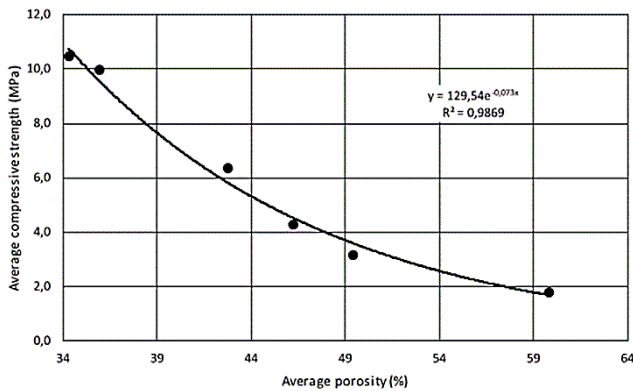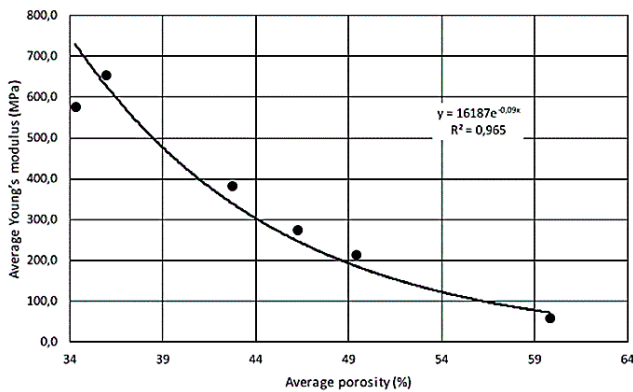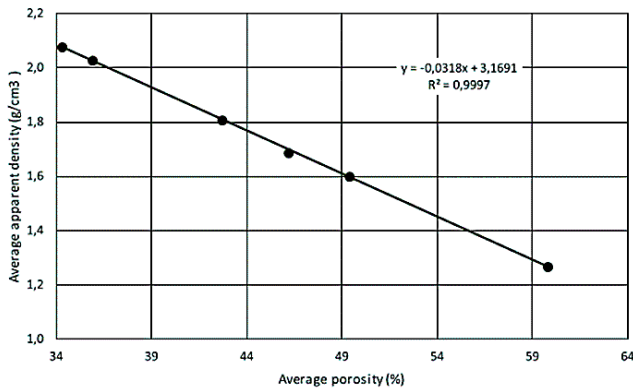| Sample	Average apparent density, g/cm³	Total porosity, %	Compressive strength, MPa	Young's modulus, MPa
S1	2.03	35.9	10	655
S2	1.69	46.2	4.3	275
S3	2.08	34.3	10.5	579
S4	1.81	42.7	6.4	385
S5	1.60	49.4	3.2	215
S6	1.27	59.8	1.8	61

Figure 3 – Average visible density, compressive strength and porosity of samples S3, S4, S5 and S6
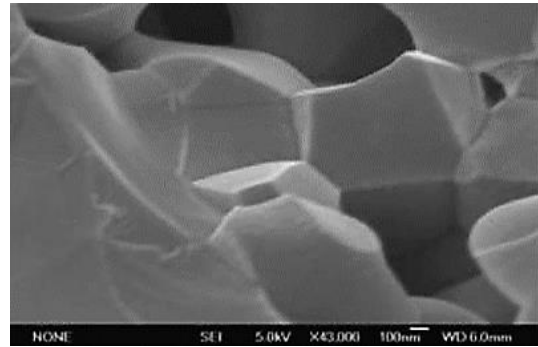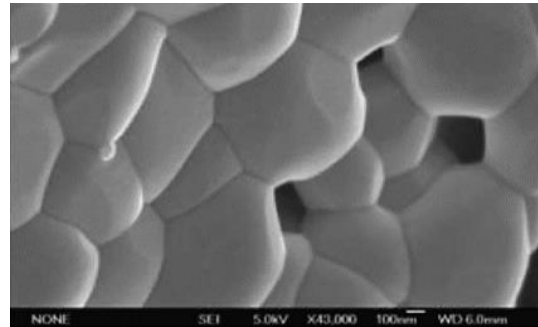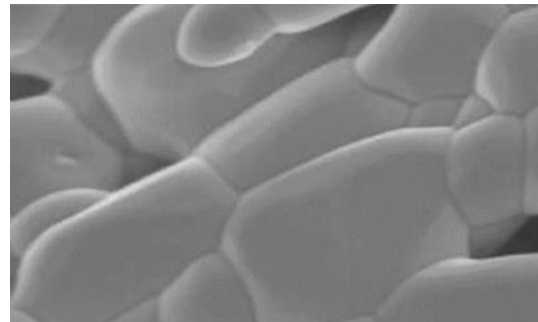

a

b

c

Figure 4 – Dependence of compressive strength, Young's modulus, and average apparent density on porosity

a

b

c
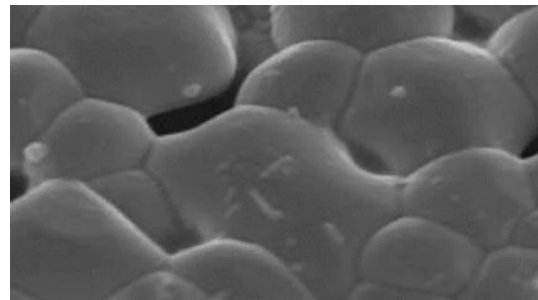
d

Figure 5 – Microphotographs of samples
3 (a), 4 (b), 5 (c) and 6 (d)

Figure 5 shows images of samples 3–6. With fewer voids shown in Figure 5 a, sample 3 with a longer mixing time has lower porosity and higher density than sample 4 (Figure 5 b). Larger crystal sizes and fewer particle boundaries with more uniform particles visible in sample 3 indicate higher crystallinity. The same results were obtained by comparing micrographs of samples 5 and 6, as shown in Figures 6 c–d. Increasing the mixing time gives a more uniform suspension and increases the crystallinity of the porous structure.

The effect of the concentration of hydroxylapatite on porosity, compressive strength, and crystallinity was evaluated; samples 2, 3, and 5 were compared with material concentrations of 44, 42, and 38 % by weight, respectively.
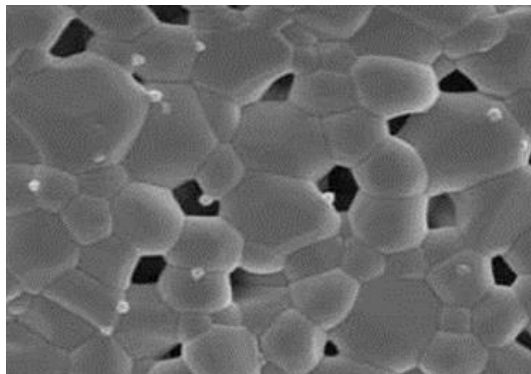
a
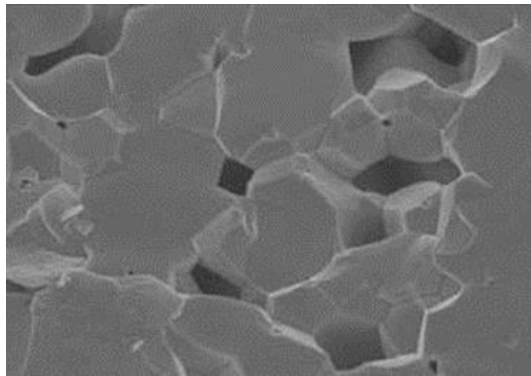
b

c

Figure 6 – Micrographs of samples: a – 2 samples (44 wt. %); b – 3 samples (42 wt. %); c – 5 samples (38 wt. %)

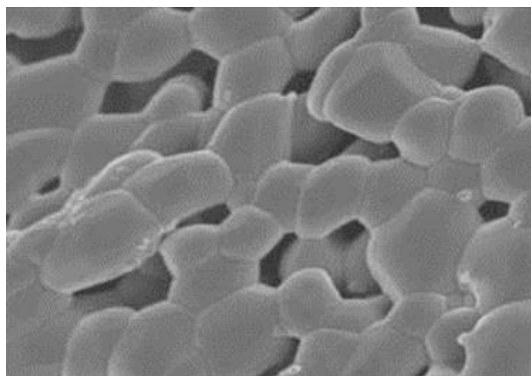From the images in Figure 6, with an increase in the concentration of hydroxyapatite from 38 to 42 % of the mass fraction, the time became more interconnected with denser and thicker pore walls, which indicates a higher density.

Glass-ceramic materials were prepared using nanostructured BHA (or SCPM) powders and sodium borosilicate glass with a weight ratio of 0.46:1. Powder mixes for SCP/glass composites were prepared by mixing sodium borosilicate glass and SCPM powders ($Ca_{10}(PO_4)_6(OH)_2$, $Ca_4(PO_4)_2O$ and $Ca_2P_2O_7$) (less than 160 μm). Samples with a diameter of 3 g and 15 mm were prepared by dry pressing under 150 MPa and sintering at 800 °C for all investigated composites. The resulting SCP powder had the composition $Ca_{10}(PO_4)_6(OH)_2$, β-tribasic calcium phosphate (β-TCP, β-$Ca_3(PO_4)_2$), tetrabasic calcium phosphate (TTCP, $Ca_4(PO_4)_2O$), calcium pyrophosphate (CPP, $Ca_2P_2O_7$).

Table 6 shows the apparent density of SCP. The apparent density is significantly influenced by the particle size of the original mixture and the type of calcium phosphate. SCP/glass is dominated by open porosity. This is due to the launched processes of phase formations in synthetic calcium phosphates during sintering, accompanied by gas formation, leading to the resulting porosity structure.

Table 6 – Number of pores, solubility, and pH change in the material after 48 and 168 hours

Parameter	SCP/glass
Open porosity	24.1 %
Closed porosity	10.4 %
Density	1.75 g/cm³
pH after 48 h	10.2
pH after 168 h	9.5
Solubility after 2 days	0.036 wt. %
Solubility after 5 days	0.054 wt. %

The apparent density is influenced by both the particle size of the feed mixture and the type of calcium phosphate. In determining the solubility in vitro, the permeability of the porous structure is also essential, which depends, instead, on the open porosity, which is effective in impregnating the material, and the design of capillary-porous channels, characterized by high crimp than on the porosity in general and the pore structure. The permeability of a structure is determined by the coefficient of permeability, which affects the rate of mass transfer when determining the rate of dissolution in vitro. The average diameter of the pore channel, established by studying the microstructure and pore size distribution, is 8.83 μm for SCP/glass. The results obtained in this work are consistent with previous studies [45].

There are many methods for making porous ceramic materials. The pore morphology can be controlled using the size of the initial powder and sintering parameters - temperature, time, pressure. Studies of various materials based on hydroxyapatite have shown that the higher the sintering rate of the material powder, the more apparent density is formed in the final material, and this leads to a higher compressive strength. It was found that increasing the mixing time increased the compressive strength and apparent density but decreased the porosity, because the longer the mixing time leads to the destruction of agglomerates, and the slurry becomes more homogeneous. There are various technologies for the manufacture of bone substitutes (electrospinning and freeze-drying). In milled bioceramics, the pore size can be reduced by increasing the temperature.

5 Conclusions

The study of the porosity of materials for biomedicine has always received considerable attention. Porosity plays an essential role in the process of introducing bone substitutes. A large and interconnected macroporosity is required for bone ingrowth to occur throughout the entire volume. Traditional methods generate random pores. New technologies for processing scaffolds allow the production of porous materials with improved mechanical properties. Since the advent of additive manufacturing technologies, triple periodic minimal surfaces (TPMS) have served as a promising tool for designing microstructures due to their superior intrinsic characteristics such as interconnection, tortuosity, and high surface-to-volume ratio.

The use of a liquid blowing agent creates scaffolds with lamellar morphology with well-defined pore connectivity. The foaming process uses dissolved gas at elevated pressure or a chemical that produces gaseous decomposition products. Rapid prototyping methods provide control over the fabrication of frameworks with reproducible porosity and specific relationships, geometry, orientation, and pore size. The SCPL method helps produce materials with controlled pore sizes and shapes. During freeze-drying, there are no harmful solvents, and it is possible to clarify the morphology of the frameworks.

Various parameters can control pore sizes during the manufacturing process (temperature, sintering speed, and stirring time). Variations in the content of porosity, pore size, and shape are possible due to changes in various processing parameters (liquid-powder ratio, concentration, the composition of the foaming agent in the solution). The fast-sintering rate of hydroxyapatite results in higher apparent density and high compressive strength. Increasing mixing time increases compressive strength and apparent density but decreases porosity. Also, an increase in the mixing period leads to the destruction of agglomerates, and the resulting suspension becomes more homogeneous. As the concentration of hydroxyapatite increases, the pores become more interconnected with denser and thicker pore walls.

References

1. Sukhodub, L. F., Diadiura, K. O. (2018). Design and fabrication of polymer-ceramic nanocomposites materials for bone tissue engineering. *Journal of Nano- and Electronic Physics*, Vol. 10(6), 06003(11pp), doi: 10.21272/jnep.10(6).06003.

2. Bouler, J. M., Pilet, P., Gauthier., O. (2017). Verron biphasic calcium phosphate ceramics for bone reconstruction: A review of biological response. *Acta Biomaterialia*, Vol. 53, pp. 1–12, doi: 10.1016/j.actbio.2017.01.076.

3. Rustom, L., Boudou, T., Lou, S., Pignot-Paintrand, I., Nemke, B. W., Lu, Y., Markel,M. D., Picart, C., Johnson, A. J. W. (2016). Micropore-induced capillarity enhances bone distribution in vivo in biphasic calcium phosphate scaffolds. *Acta Biomaterialia*, Vol. 44, pp. 144–154, doi: 10.1016/j.actbio.2016.08.025.

4. Johnson, A. J. W., Herschler, B. A. (2011). A review of the mechanical behavior of CaP and CaP/polymer composites for applications in bone replacement and repair. *Acta Biomaterialia*, Vol. 7(1), pp. 16–30, doi: 10.1016/j.actbio.2010.07.012.

5. Miclăuş, T., Valla, V., Koukoura, A., Nielsen, A. A., Dahlerup, B., Tsianos, G.-I., Vassiliadis, E. (2020). Impact of design on medical device safety. *Therapeutic Innovation and Regulatory Science*, Vol. 54(4), pp. 839–849, doi: 10.1007/s43441-019-00022-4.

6. Babaie, E., Bhaduri, S. B. (2017). Fabrication aspects of porous biomaterials in orthopedic applications: A review. *ACS Biomater. Sci. Eng*, Vol. 4(1), pp. 1–39, doi: 10.1021/acsbiomaterials.7b00615.

7. Diez-Escudero, A., Espanol, M., Ginebra, M. P. (2020). Synthetic bone graft substitutes: Calcium-based biomaterials. *Dental Implants and Bone Grafts*, Woodhead Publishing, pp. 125–157.

8. Ternero, F., Rosa, L. G., Urban, P., Montes, J. M., Cuevas, F. G. (2021). Influence of the total porosity on the properties of sintered materials – A review. *Metals*, Vol. 11(5), 730, doi: 10.3390/met11050730.

9. Gibson, L. J., Ashby, M. F. (1999). *Cellular Solids: Structure and Properties*. Cambridge University Press.

10. Rho, J. Y., Kuhn-Spearing, L., Zioupos, P. (1998). Mechanical properties and the hierarchical structure of bone. *Medical Engineering and Physics*, Vol. 20(2), pp. 92–102, doi: 10.1016/S1350-4533(98)00007-1.

11. Cordell, J. M., Vogl, M. L., Johnson, A. J. W. (2009). The influence of micropore size on the mechanical properties of bulk hydroxyapatite and hydroxyapatite scaffolds. *Journal of the Mechanical Behavior of Biomedical Materials*, Vol. 2(5), pp. 560–570, doi: 10.1016/j.jmbbm.2009.01.009.

12. Prokopiev, O., Sevostianov, I. (2006). Dependence of the mechanical properties of sintered hydroxyapatite on the sintering temperature. *Materials Science and Engineering: A*, Vol. 431(1-2), pp. 218–227, doi: 10.1016/j.msea.2006.05.158.

13. Prokopiev, O., Sevostianov, I. (2006). On the possibility of approximation of irregular porous microstructure by isolated spheroidal pores. *International Journal of Fracture*, Vol. 139(1), pp. 129–136, doi: 10.1007/s10704-006-8370-9.

14. Lutzweiler, G., Halili, A. N., Vrana, N. E. (2020). The overview of porous, bioactive scaffolds as instructive biomaterials for tissue regeneration and their clinical translation. *Pharmaceutics*, Vol. 12(7), pp. 602, doi: 10.3390/pharmaceutics12070602.

15. Montazerian, H., Davoodi, E., Asadi, M., Kadkhodapour, J. (2017). Porous scaffold internal architecture design based on minimal surfaces: A compromise between permeability and elastic properties. *Mater. Des.*, Vol. 126, pp. 98–114, doi: 10.1016/j.matdes.2017.04.009.

16. Bobbert, F. S. L., Lietaert, K., Eftekhari, A. A., Pouran, B., Ahmadi, S. M., Weinans, H., Zadpoor, A. A. (2017). Additively manufactured metallic porous biomaterials based on minimal surfaces: A unique combination of topological, mechanical, and mass transport properties. *Acta Biomaterialia*, Vol. 53, pp. 572–584, doi: 10.1016/j.actbio.2017.02.024.

17. Babaie, E., Ren, Y., Bhaduri, S. B. (2016). Microwave sintering of fine grained MgP and Mg substitutes with amorphous tricalcium phosphate: Structural, and mechanical characterization. *J. Mater. Res.*, Vol. 31(08), pp. 995–1003, doi: 10.1557/jmr.2016.84.

18. Sebastian, T., Preisker, T. R., Gorjan, L., Graule, T., Aneziris, C. G., Clemens, F. J. (2020). Synthesis of hydroxyapatite fibers using electrospinning: A study of phase evolution based on polymer matrix. *Journal of the European Ceramic Society*, Vol. 40(6), pp. 2489–2496, doi: 10.1016/j.jeurceramsoc.2020.01.070.

19. Faridi-Majidi, R., Nezafati, N., Pazouki, M., Hesaraki, S. (2017). The effect of synthesis parameters on morphology and diameter of electrospun hydroxyapatite nanofibers. *J Aust Ceram Soc.*, Vol. 53, pp. 225–233, doi: 10.1007/s41779-017-0028-8.

20. Czechowska, J., Zima, A., Siek, D., Ślósarczyk, A. (2018). Influence of sodium alginate and methylcellulose on hydrolysis and physicochemical properties of α- TCP based materials. *Ceramics International*, Vol. 44(6), pp. 6533–6540, doi: 10.1016/j.ceramint.2018.01.055.

21. Januariyasa, K., Yusuf, Y. (2020). Porous carbonated hydroxyapatite-based scaffold using simple gas foaming method. *Journal of Asian Ceramic Societies*, Vol. 8(3), pp. 634–641, doi: 10.1080/21870764.2020.1770938.

22. Li, X., Deng, Y., Chen, X., Xiao, Y., Fan, Y., Zhang, X. (2016). Gelatinizing technology combined with gas foaming to fabricate porous spherical hydroxyapatite bioceramic granules. *Materials Letters*, Vol. 185, pp. 428–431, doi: 10.1016/J.MATLET.2016.09.036.

23. Mamat, N., Darus, F., Md Isa, R., Jaafar, M., Kawashita, M. (2017). Hierarchical bioceramic scaffold for tissue engineering: A review. *International Journal of Polymeric Materials and Polymeric Biomaterials*, Vol. 66(17), pp. 877–890, doi: 10.1080/00914037.2017.1291507.

24. Wu, Z., Zhou, Z., Hong, Y. (2018). Isotropic freeze casting of through-porous hydroxyapatite ceramics. *Journal of Advanced Ceramics*, Vol. 8(2), pp. 256–264, doi: 10.1007/s40145-018-0312-2.

25. Mondal, S., Hoang, G., Manivasagan, P., Moorthy, M. S., Nguyen, T. P., Phan, T. T. V., Kim, H. H., Kim, M. H., Nam, S. Y., Oh, Y. (2018). Nano-hydroxyapatite bioactive glass composite scaffold with enhanced mechanical and biological performance for tissue engineering application. *Ceramics International*, Vol. 44 (13), pp. 15735–15746, doi: 10.1016/j.ceramint.2018.05.248.

26. Yuan, B., Zhou, S.-Y., Chen, X.-S. (2017). Rapid prototyping technology and its application in bone tissue engineering. *Journal of Zhejiang University-Science B*, Vol. 18(4), pp. 303–315, doi: 10.1631/jzus.B1600118.

27. Truneca, M., Chlup, Z. (2017). Subtractive manufacturing of customized hydroxyapatite scaffolds for bone regeneration. *Ceramics International*, Vol. 43(14), pp. 11265–11273, doi: 10.1016/j.ceramint.2017.05.177.

28. Sapkal, P. S., Kuthe, A. M., Kashyap, R. S., Nayak, A. R., Kuthe, S. A., Kawle, A. P. (2016). Indirect fabrication of hydroxyapatite/b-tricalcium phosphate scaffold for osseous tissue formation using additive manufacturing technology. *J Porous Mater*, Vol. 23(6), pp. 1567–1574, doi: 10.1007/s10934-016-0217-9.

29. Hassanajili, S., Pour, A. K., Oryan, A., Talaei-Khozani, T. (2019). Preparation and characterization of PLA/PCL/HA composite scaffolds using indirect 3D printing for bone tissue engineering. *Materials Science and Engineering C*, Vol. 104, 109960, doi: 10.1016/j.msec.2019.109960.

30. Houben, A., Van Hoorick, J., Van Erps, J. A., Thienpont, H., Van Vlierberghe, S., Dubruel, P. (2017). Indirect rapid prototyping: opening up unprecedented opportunities in scaffold design and applications. *Ann. Biomed. Eng*, Vol. 45(1), pp. 58–83, doi: 10.1007/s10439-016-1610-x.

31. Hui, D., Goodridge, R. D., Scotchford, C. A., Grant, D. M. (2018). Laser sintering of nano-hydroxyapatite coated polyamide 12 powders. *Additive Manufacturing*, Vol. 22, pp. 560–570, doi: 10.1016/j.addma.2018.05.045.

32. Khallok, H., Elouahli, A., Ojala, S., Keiski, R. L., Kheribech, A., Hatim, Z. (2020). Preparation of biphasic hydroxyapatite/ β-tricalcium phosphate foam using the replication technique. *Ceramics International*, Vol. 46(14), pp. 22581–22591, doi: 10.1016/j.ceramint.2020.06.019.

33. Wong, W. Y., Noor, A.-F. M., Othman, R. (2016). Sintering of beta-tricalcium phosphate scaffold using polyurethane template. *Key Engineering Materials*, Vol. 694, pp. 94–98, doi: 10.4028/www.scientific.net/KEM.694.94.

34. Gandhimathi, C., Venugopal, J. R., Ramakrishna, S., Srinivasan, D. K. (2018). Electrospun-electrosprayed hydroxyapatite nanostructured composites for bone tissue regeneration. *Journal of Applied Polymer Science*, Vol. 135(42), 46756, doi: 10.1002/app.46756.

35. Seyedmajidi, S., Seyedmajidi, S., Alaghehmand, H., Hajian-Tilaki, K., Haghanifar, S., Zabihi, E., Rayabnia, R., Seyedmajidi, M. (2018). Synthesis and characterization of hydroxyapatite/bioactive glass nanocomposite foam and fluorapatite/bioactive glass nanocomposite foam by gel casting method as cell scaffold for bone tissue. *Eurasian J Anal Chem*, Vol. 13(3), em17, doi: 10.29333/ejac/85078.

36. Miola, M., Verne, E., Vitale-Brovarone, C., Baino, F. (2016). Antibacterial bioglass-derived scaffolds: Innovative synthesis approach and characterization. *International Journal of Applied Glass Science*, Vol. 7(2), pp. 238–247, doi: 10.1111/ijag.12209.

37. Shao, H., He, J., Lin, T., Zhang, Z., Zhang, Y., Liu, S. (2018). 3D gel-printing of hydroxyapatite scaffold for bone tissue engineering. *Ceramics International*, Vol. 45(1), pp. 1163–1170, doi: 10.1016/j.ceramint.2018.09.300.

38. Gomes, D. S., Santos, A. M. C., Neves, G. A., Menezez, R. R. (2019). A brief review on hydroxyapatite production and use in biomedicine. *Cerâmica*, Vol. 65(374), pp. 282–302, doi: 10.1590/0366-69132019653742706.

39. Siddiqui, H. A., Pickering, K. L., Mucalo, M. R. (2018). A review on the use of hydroxyapatite carbonaceous structure composites in bone replacement materials for strengthening purposes materials. *Materials (Basel)*, Vol. 11(10), 1813, doi: 10.3390/ma11101813.

40. Kamrun, N. U., Shovon, B., Rajib, C. D., Shujit, C. P, Shukanta, B., Muhammed, Y. M., Sydul, I. M. D. (2017). Characterization of beta-tricalcium phosphate (β- TCP) produced at different process conditions. *J Bioengineer and Biomedical Sci*, Vol. 7(221), doi: 10.4172/2155-9538.1000221.

41. Abe, Y., Kobatake, R., Okazaki, Y., Oki, Y., Naito, Y., Prananingrum, W., Tsuga, K. (2017). Novel development of phosphate treated porous hydroxyapatite. *Materials*, Vol. 10(12), 1405. doi: 10.3390/ma10121405.

42. Karyasa, I. W. (2021). Developing renewable thermo-hydrothermic bioinorganic materials from bone wastes of slaughterhouses. *Journal of Physics: Conference Series*, Vol. 1869(1), 012030, doi: 10.1088/1742-6596/1869/1/012030.

43. ISO 13175-3:2012 Implants for surgery – Calcium phosphates – Part 3: Hydroxyapatite and beta-tricalcium phosphate bone substitutes.

44. Pinchuk, N., Parkhomey, O., Sych, O. (2017) In vitro investigation of bioactive glass-ceramic composites based on biogenic hydroxyapatite or synthetic calcium phosphates. *Nanoscale Research Letters*, Vol. 1(111), doi: 10.1186/s11671-017-1895-1.

45. Parkhomei, O. R., Pinchuk, N. D., Sych, O., Tomila, T. (2016). Structural and mechanical properties of bioactive glass–ceramic composites. *Powder Metallurgy and Metal Ceramics*, Vol. 55 (3-4), doi: 10.1007/s11106-016-9792-1.